Searching for seismic scattering off mantle interfaces between 800 km and 2000 km depth

John C. Castle[1] and Rob D. van der Hilst[2]

Department of Earth, Atmospheric and Planetary Sciences, Massachusetts Institute of Technology, Cambridge, Massachusetts, USA

Received 24 August 2000; revised 23 March 2002; accepted 28 March 2002; published 13 February 2003.

[1] We systematically examined seismic data from deep earthquakes in the western and northwestern Pacific, Tonga/Fiji, and South America for signs of sharp gradients in seismic properties that could represent either a mineralogical phase change or the boundary between geochemical reservoirs in the Earth's lower mantle. This involved the stacking of short-period, vertical component teleseismic waveforms from the dense Pacific Northwest Seismic Network and searching for evidence of *S*-to-*P* conversions at sharp mantle structures between 800 and 2000 km depth. With these data, we estimate we should be able to detect seismic discontinuities with $\Delta V_s > 2\%$, transition width <20 km, and limited local topography. Using data from over 45 earthquakes, we found no evidence of a horizontal global discontinuity, neither near 920 km nor near 1700 km, beneath the four convergent margins studied here. Consistent with previous results, we detected a deep structure with topography near 1600 km beneath the Marianas region. Because we observed the signal over a large geographical region beneath the Marianas (10°N to 20°N), it is likely a coherent local structural and not a point source. The absence of such a structure beneath the northwest Pacific, the Tonga/Fiji region, or South America, argues against a global feature near 1600 km depth, however. The lack of convincing and consistent scattering suggests that no composition boundary or thermal boundary layer exists between 800 to 2000 km depth beneath the convergent zones studied that has $\Delta V_s < 2\%$, locally limited topography, and a transition interval <20 km. *INDEX TERMS:* 8124 Tectonophysics: Earth's interior—composition and state (8105); 8130 Tectonophysics: Evolution of the Earth: Heat generation and transport; 8121 Tectonophysics: Dynamics, convection currents and mantle plumes; 7207 Seismology: Core and mantle; *KEYWORDS:* mantle, chemistry, seismology, composition, discontinuity heat

Citation: Castle, J. C., and R. D. van der Hilst, Searching for seismic scattering off mantle interfaces between 800 km and 2000 km depth, *J. Geophys. Res.*, *108*(B2), 2095, doi:10.1029/2001JB000286, 2003.

1. Introduction

[2] The distinctly different geochemical signatures of ocean island basalts (OIB) and mid-ocean ridge basalts (MORB) suggest that chemically distinct reservoirs exist within the Earth's mantle [e.g., *Hofmann*, 1997]. One reservoir would supply MORBs, while a distinct, or several distinct, reservoirs could feed OIBs. The heat flow generated by a mantle with a potassium, thorium, and uranium content equal to that of the MORB source would be considerably less than the heat flow currently observed, suggesting the existence of an isolated mantle reservoir enriched in radiogenic elements [e.g., *Becker et al.*, 1999; *Kellogg et al.*, 1999a]. The mid-ocean ridges would then sample the depleted reservoir, whereas the enriched reservoir(s) would have remained largely unsampled by the ridges. Unfortunately, several uncertainties exist. The heat flux from the core into the mantle has remained enigmatic, and geochemical data and heat flow constraints confine neither the location nor the geometry of the geochemical reservoirs. Moreover, it is not required that the geochemical and radiogenic reservoirs are identical [e.g., *Davies*, 1999; *Albarède and van der Hilst*, 1999; *Tackley*, 2000] nor is it obvious if and how they could be detected seismologically.

[3] Dividing the mantle into geochemical reservoirs with a reservoir boundary at 660 km depth has long been one hypothesis; however, this idea has become virtually untenable with the tomographic evidence for slabs flowing across the 660 km discontinuity into the lower mantle [e.g., *Creager and Jordan*, 1986; *van der Hilst et al.*, 1997; *Grand et al.*, 1997]. However, downwelling slabs may supply the lowermost mantle with a unique geochemical signature [e.g., *White and Hofmann*, 1982; *Christensen and Hofmann*, 1994], although this process does probably not produce sufficient enrichment to satisfy the mass balances [*Albarède and van der Hilst*, 2002]. Recent hypotheses to

[1]Now at Rosetta Inpharmatics, Seattle, Washington, USA.

[2]Now at Department of Geophysics, Institute of Earth Sciences, Utrecht University, Utrecht, Netherlands.

0148-0227/03/2001JB000286$09.00

explain the geochemical and heat flow observations include both reservoirs of undepleted, chemically distinct material in viscous blobs [*Becker et al.*, 1999] and a chemically distinct reservoir starting at a depth deeper than 660 km [*van der Hilst et al.*, 1998; *Tackley*, 1998; *Kellogg et al.*, 1999a; *van der Hilst and Kárason*, 1999; *Davaille*, 1999] (see *Albarède and van der Hilst* [1999] and *Tackley* [2000] for reviews) (Figure 1).

[4] One-dimensional (1-D) velocity profiles such as iasp91 [*Kennett and Engdahl*, 1991] and PREM [*Dziewonski and Anderson*, 1981] represent laterally averaged earth structure and model the mantle from 760 to 2740 km depth as a region of smoothly increasing wave speeds and densities. Taken at face value, this implies that either (1) neither mineralogical phase changes nor chemical changes occur within this depth range; (2) if a change does occur, the resulting wave speed and density changes are small enough to have avoided detection; or (3) the model parameterization (i.e., low order polynomial expansion) precludes proper representation of steep but otherwise subtle gradients in the lower mantle.

[5] Neither the blob nor any of the deep geochemical reservoir hypotheses would necessarily predict a distinct structure in radial earth profiles. Mantle flow would control the locations of blobs throughout the mantle and these structures need not contribute to a signal in 1-D seismic profiles. A deep geochemical reservoir would be stable at the base of the mantle only if its intrinsic density is greater than the overriding layer [*Sleep*, 1988]. If the deep reservoir is also enriched in radiogenic elements it would heat up and either remain marginally denser than the overlying mantle [*Tackley*, 1998; *Kellogg et al.*, 1999a], with a possibly oscillatory time dependence [*Davaille*, 1999], or become positively buoyant [*Forte and Mitrovica*, 2001], in which case, however, it is hard to explain the long residence times implied by geochemical mass balancing [e.g., *Hofmann*, 1997]. In a convecting mantle, an inter-layer boundary with a small density contrast could develop considerable dynamic topography (>100 km) and would not necessarily be discernible in one dimensional (1-D) velocity models.

[6] Three-dimensional tomographic inversions of global travel times, such as the first arriving *P* phase, could reveal different mantle domains if the volumetric wave speeds are different, such as the joint use of *P* and *S* wave inversions for variations in composition or temperature [e.g., *Kennett et al.*, 1998; *Masters et al.*, 2000; *Saltzer et al.*, 2001; *Forte and Mitrovica*, 2001]. While these studies have begun to reveal compositional heterogeneity in the lowermost mantle, the location of and total volume of the mantle involved in these distinct domains is still highly uncertain. Moreover, 3-D tomographic imaging with transmitted body waves is not well suited to characterizing the depth, orientation, and impedance contrast of any interfaces between such domains.

[7] In contrast to transmission topography, "scattering tomography" seeks to image sharp structures along ray paths, such as a boundary between geochemical reservoirs or slab debris settling atop a boundary. Scattered, reflected, and converted phases have been used to image structures in the transition zone [e.g., *Castle and Creager*, 1998] and in the lowermost mantle [e.g., *Hedlin et al.*, 1997]. Furthermore, local scattering structures have been imaged at 920 km depth under the Indonesian slab [*Kawakatsu and Niu*, 1994], at 1000 km depth near the Izu-Bonin trench [*Niu and Kawakatsu*, 1997; *Castle and Creager*, 1999], and at 1600 km in the Marianas region [*Kaneshima and Helffrich*, 1998, 1999]. To search for signs of wave field scattering indicative of lower mantle structure in the depth range 800–2000 km, we examined short-period, vertical component seismograms from deep earthquakes beneath the convergent margins of the western and northwestern Pacific, Tonga/Fiji, and South America recorded at the dense Pacific Northwest Seismic Network (PNSN). By stacking and migrating the data on an earthquake-by-earthquake basis we were able to examine specific regions of the lower mantle without averaging over large volumes.

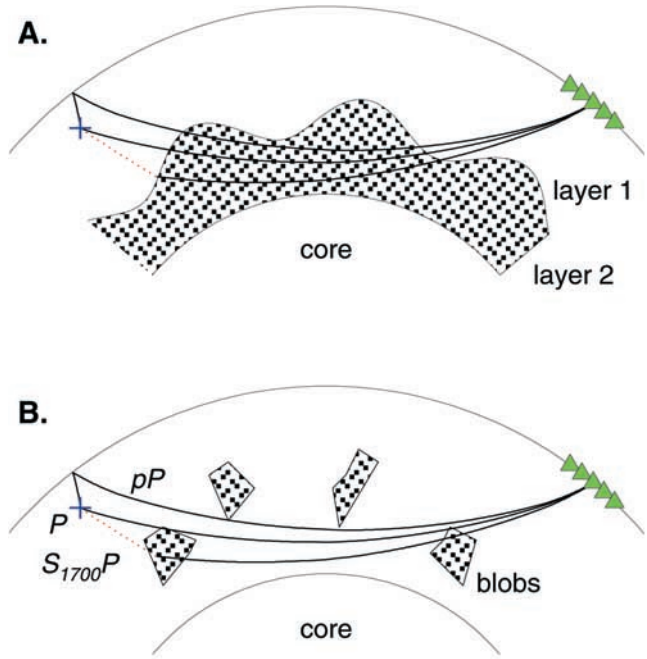

Figure 1. Cartoon showing two different models incorporating distinct geochemical reservoirs in the mantle. (a) Two-layer mantle model vertically divided at some depth, possibly near 1700 km, in the lower mantle with considerable topography [*Kellogg et al.*, 1999a]. (b) Homogeneous whole mantle containing chemically heterogeneous blobs of varying size [*Becker et al.*, 1999]. Superimposed on both models are the schematic ray paths of the *P*, *pP*, and $S_{1700}P$ for a 500 km deep earthquake recorded at 80° distance.

2. Searching for Deep Structure

[8] We considered several methods in our search of blobs or subhorizontal discontinuities in the middle mantle (800–2000 km). Similar to studies of the 410 and 660 discontinuities [e.g., *Shearer*, 1991] we have stacked global data and searched for precursors to phases such as *PP* and *SS*. Unfortunately, precursors that would come from middle mantle depths arrive simultaneously with other phases and we detected no convincing precursor off structure between 660 and 2000 km depth. Similarly, stacked *ScS* reverberations sampling the western Pacific region show no signs of a constant-depth interface at large depth [*Revenaugh and Jordan*, 1991]. These results render it unlikely that a horizontal global discontinuity exists in the middle mantle.

However, depending on the frequency of waves used, the signal from a structure with over ~50 km of vertical topography would stack incoherently and not be discernible.

[9] We also employed methods that examine specific geographical regions of the mantle. Receiver functions use *P*-to-*S* conversions under seismic stations to image deep structures, such as the 410 and 660-km discontinuities [e.g., *Vinnik et al.*, 1997]. Unfortunately, the surface reflected *PP* arrives in the time window expected for *P*-to-*S* conversions at depths between 1000 and 2000 km, and the larger amplitude of *PP* would mask any signals from a deeper structure.

[10] Previously, we, and others, have used *S*-to-*P* phase conversions successfully to image the 660-km discontinuity and deeper structures [e.g., *Castle and Creager*, 1999]. The phase $S_{660}P$ leaves an earthquake as an *S* wave, converts to a *P* wave at the 660-km discontinuity, and continues to the receivers following a path similar to the direct *P* wave. On individual records, the near-receiver reverberations are much larger than the $S_{660}P$ signal. But unlike near-receiver reverberations, the $S_{660}P$ signal arrives coherently across the entire network. Thus by stacking seismograms from dense seismic networks one can identify $S_{660}P$ and determine its arrival time, slowness, and back-azimuth. Combined with knowledge of the earthquake hypocenter and the seismic wave speeds, the discontinuity depth can be inferred from the $S_{660}P$-*P* delay time. Similarly, one can search for structure at greater depths (S_XP) and, by looking for arrivals off the great circle path, search for nonhorizontal, dipping structures.

[11] While this method has been successfully used with data from shallow earthquakes (<50 km) [*Castle and Creager*, 1998], the coda from earlier arriving depth phases, *pP* and *sP*, lowers the detection level of potential S_XP signals. An advantage of this method is the good slowness and azimuth resolution that one can obtain with large numbers of seismograms from a dense, large aperture seismic network. Importantly, if the mantle density increases while the velocity decreases across an interface, the impedance change could potentially be zero. Unlike reflected waves, however, *S*-to-*P* conversions are essentially sensitive to ΔV_s only and not the impedance change [*Castle and Creager*, 2000]. Finally, the method does not average over wide regions but instead provides an image of local structure, which is important for imaging a boundary that may have considerable topography. While a boundary with local dip >30° in an unfavorable orientation would go undetected, by examining regions individually, we should be able to detect regions with local dips <30°.

3. Data and Methodology

3.1. Processing

[12] Figure 2 shows seismograms from a Tonga/Fiji earthquake recorded at PNSN. To focus on small-amplitude phases in the *P* coda we used the procedure employed by [*Castle and Creager*, 2000]: band-pass filter the data at 2–5 s, align them on the P wave, delete signals with low signal-to-noise ratios, and phase-weight stack [*Schimmel and Paulssen*, 1997]. Nonhorizontal, 3-D structure on a discontinuity will generate seismic phases that propagate out of the great circle path and at slownesses different from the *P*-wave slowness and back-azimuth. By adding time shifts to each seismogram based on its distance and azimuth and then stacking the data, we used the seismic network as an antenna looking into the Earth to search for phases arriving from different directions. We have previously been able to identify signals coming from structures dipping at angles as steep as 30° [see *Castle and Creager*, 1998].

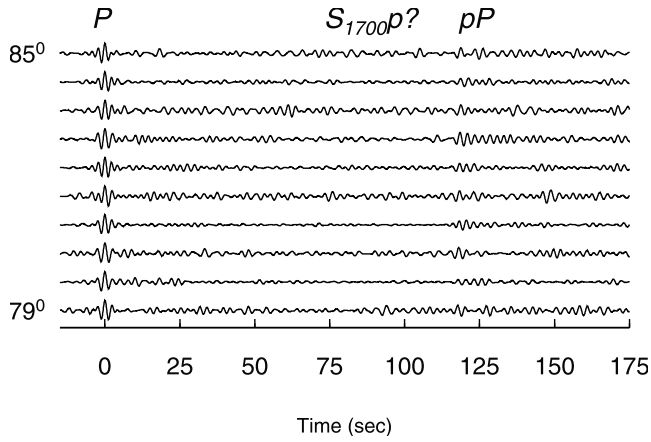

Figure 2. Ten of the 109 seismograms from earthquake 41 in Tonga/Fiji. The seismograms have been filtered and, without further processing, aligned on the *P* wave. Only the *P* and *pP* phases are visible.

3.2. Synthetic Data

[13] Figure 3 shows synthetic seismograms and stacks of them at various slownesses along the earthquake/receiver great circle path (a vespegram). For this event, event 1 in Table 1, *pP* arrives about 125 s after the *P* wave at a slowness 0.6 s deg^{-1} greater than the *P* wave, which is consistent with the shallower turning point. Figures 3c and 3d show the slowness and azimuth energy arriving in a 20 s time window centered on the *P* wave and in a time window from the theoretical $S_{1600}P$ time to the $S_{1900}P$ time. Note that in all of the following figures the second time window always stops at least 10 s before *pP* to avoid interference from this signal.

[14] The synthetic seismograms were created with the WKBJ algorithm [*Chapman et al.*, 1988], using the iasp91 velocity model [*Kennett and Engdahl*, 1991] and the PREM density model [*Dziewonski and Anderson*, 1981], both modified to include a 2% jump at 1700 km. We verified that other models, such as only PREM or ak135 [*Kennett et al.*, 1995], yield similar results. The synthetics included the *P*, *pP*, $s_{410}P$, $p_{410}P$, $S_{660}P$, and $S_{1700}P$ phases. $s_{410}P$ is an upgoing *S* wave that reflects and converts off of the 410-km discontinuity above the earthquake. Similarly, $p_{410}P$ leaves the earthquake as an upgoing traveling *P* wave that reflects at 410 km. $S_{660}P$ is not seen for deep earthquakes since it arrives within 5 s after the *P* wave.

[15] Normalizing amplitudes from earthquake to earthquake is often frustrating. Confounding this affect is that a given earthquake will differentially emit *P* and *S* energies. With the risk of amplifying noise, we initially normalized all seismograms on the *P* wave and afterwards normalized later time windows on the expected amount of *S* wave energy to better show small amplitude arrivals. The time

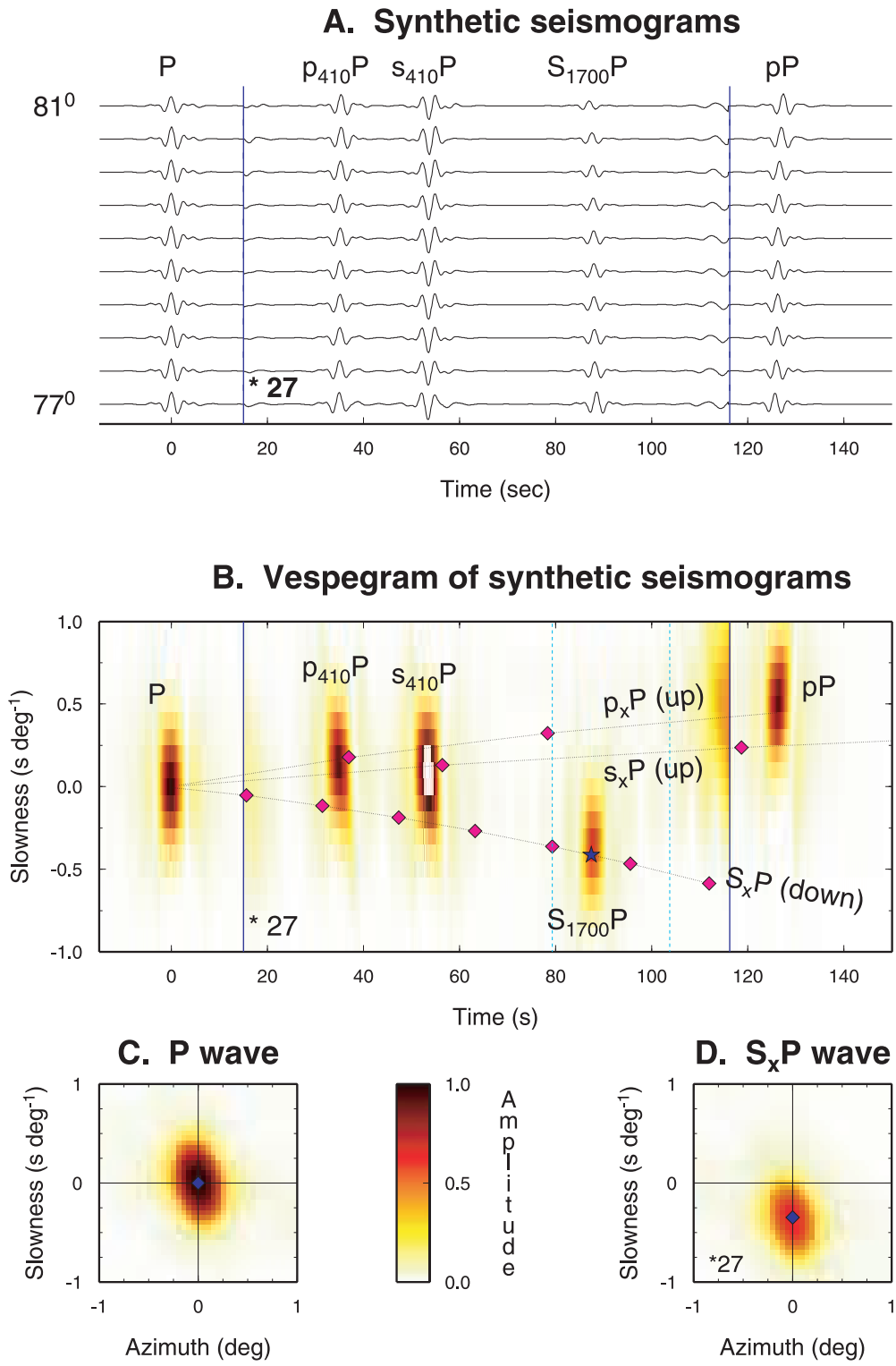

Figure 3. WKBJ synthetic seismograms. The wave speed model included a 2% jump at 1700 km depth. (a) Ten synthetic seismograms modeled after earthquake 1. The amplitudes between the solid vertical lines have been increased by 27 (see text). (b) A vespegram showing the stacked data for time versus slowness. Light lines plot the expected arrival times and slowness of upgoing p_xP phases, upgoing s_xP phases, and downgoing S_XP phases. Diamonds mark the arrival times and slownesses of conversions off of 200 and 400 km (p_xP and s_xP) and 800, 1000, 1200, 1400, 1600, 1800, and 2000 ($S_{xx}P$). (c) The slowness an azimuth of energy arriving in a time window around the P wave. Dark blue diamonds mark the slowness and azimuth of the largest arrival in the time window. (d) As for Figure 3c but for a time window from the theoretical $S_{1600}P$ arrival time to the earlier of the $S_{1900}P$ arrival time or 10 s before the pP phase.

Table 1. Deep Earthquakes Recorded at PNSN[a]

Event	Date	Location, °N	Location, °E	Depth, km	M_b	Number of Stations	Δ deg	Radiation Pattern $S_{1700}P$	Radiation Pattern P	Radiation Pattern Ratio
				Marianas Earthquakes to PNSN						
1	23 Aug. 1995	18.8	145.3	608	6.0	125	79	0.69	0.49	8.68
2	24 Aug. 1995	18.9	145.1	592	6.0	121	79	0.69	0.48	8.78
3	24 Aug. 1995	18.8	145.2	622	6.0	118	79	0.69	0.49	8.59
				Northwest Pacific Earthquakes to PNSN						
4	20 April 1984	50.0	148.8	591	6.0	70	56	0.16	−0.40	−2.49
5	3 Feb. 1986	27.9	139.5	530	5.8	97	76	0.79	0.73	6.67
6	11 May 1990	41.8	131.0	582	5.7	89	71	0.52	0.88	3.63
7	12 May 1990	49.0	141.9	613	6.5	80	60	0.23	−0.15	−9.23
8	5 Aug. 1990	29.5	137.7	501	6.0	102	76	0.28	0.37	4.73
9	20 Jan. 1992	27.9	139.5	502	5.8	98	76	0.51	0.33	9.47
10	21 July 1994	41.3	132.4	508	6.5	115	71	0.75	0.67	6.88
				South American Earthquakes to PNSN						
11	1 May 1985	−9.2	288.8	606	6.0	89	71	0.25	−0.55	−2.81
12	27 Oct. 1987	−28.7	297.0	615	6.0	74	91	0.73	0.50	8.84
13	6 Nov. 1987	−22.9	296.4	536	5.8	99	87	0.47	0.31	9.52
14	5 May 1989	−8.3	288.6	593	6.4	79	71	0.30	−0.65	−2.86
15	17 Oct. 1990	−11.0	289.3	599	6.7	75	73	0.37	−0.61	−3.72
16	23 June 1991	−26.8	296.7	562	6.4	102	90	0.19	−0.32	−3.57
17	10 Jan. 1994	−13.4	290.6	596	6.4	81	76	−0.51	−0.73	4.27
18	29 April 1994	−28.3	296.8	569	6.3	114	91	0.43	−0.26	−10.15
19	10 May 1994	−28.5	297.0	604	6.4	96	91	0.53	0.26	12.70
20	9 June 1994	−13.9	292.5	636	7.0	77	77	−0.63	−0.78	4.91
21	4 Nov. 1994	−9.4	288.7	591	5.8	119	71	0.16	−0.76	−1.28
22	28 Nov. 1997	−13.8	291.2	604	6.0	106	76	−0.50	−0.71	4.32
				Tonga/Fiji Earthquakes to PNSN						
23	17 Sept. 1982	−23.5	180.2	549	5.9	85	88	−0.42	0.20	−12.90
24	28 Aug. 1985	−21.0	181.1	634	6.1	100	85	0.09	−0.65	−0.82
25	21 May 1989	−17.9	181.5	593	5.7	96	82	0.49	0.26	11.81
26	16 Nov. 1989	−17.7	181.1	541	5.7	103	82	0.90	0.72	7.67
27	18 Jan. 1990	−20.8	181.6	581	6.0	62	85	−0.60	0.01	−312.66
28	17 May 1990	−25.5	178.2	602	5.9	101	90	0.22	0.98	1.37
29	26 June 1990	−22.0	180.6	594	6.0	83	86	0.13	−0.13	−6.14
30	22 July 1990	−23.6	180.1	534	5.9	103	88	0.11	0.57	1.18
31	30 Sept. 1991	−20.8	181.5	581	6.3	107	84	−0.15	−0.34	2.72
32	3 Dec. 1991	−26.5	178.8	572	6.0	41	89	0.31	0.35	5.45
33	24 April 1993	−17.8	179.9	595	6.1	68	83	0.05	0.34	0.99
34	7 Aug. 1993	−24.0	179.9	550	6.0	94	88	0.59	0.45	8.14
35	9 March 1994	−18.0	181.6	562	6.6	106	82	0.42	−0.30	−8.73
36	31 March 1994	−22.0	180.6	590	6.1	103	86	0.38	0.16	14.75
37	27 Oct. 1994	−25.8	179.4	523	5.9	72	89	0.28	0.54	3.16
38	18 Dec. 1994	−17.9	181.4	549	5.6	86	82	−0.18	0.65	−1.69
39	17 Jan. 1995	−20.9	180.9	636	5.9	106	85	0.75	0.86	5.28
40	13 April 1995	−13.5	170.6	634	6.0	98	85	0.64	0.44	8.82
41	14 Sept. 1995	−17.7	181.1	538	6.0	109	82	0.58	0.36	9.94
42	29 Oct. 1995	−21.8	180.7	610	6.0	116	86	0.59	0.38	9.38
43	5 Aug. 1996	−20.7	181.8	555	6.0	109	84	0.58	0.36	9.86
44	19 Oct. 1996	−20.4	181.6	586	6.0	111	84	0.58	0.37	9.61
45	4 Sept. 1997	−26.5	178.5	604	6.0	110	91	0.60	0.39	9.33
46	29 March 1998	−17.6	180.9	537	6.0	98	82	0.59	0.36	9.94

[a]The radiation pattern ratio column is the ratio of the ground motion at the earthquake.

window starting 15 s after the P wave to 10 s before the pP wave is amplified. We determined the amplification factor by calculating the ratio of S to P energy for a given earthquake at both the $S_{1700}P$ and P slownesses, respectively, using the USGS moment tensors [*Sipkin*, 1986] and increased the amplitudes within the time window by an empirically chosen factor of 500 divided by the S-to-P ratio. By dividing by the S-to-P ratio, the S_XP time window is amplified more for earthquakes from which we expect small S_XP arrivals. Note that this is a large amount of amplification, larger than in comparable studies, in an attempt to show any structure at the risk of amplifying noise.

[16] From this synthetic example, $S_{1700}P$ arrives ∼90 s after the P wave. $S_{1700}P$ travels along a deeper ray path (Figure 1) so that its slowness is ~ -0.5 s deg^{-1} relative to the P wave slowness. As no 3-D topography is present in this Earth model, $S_{1700}P$ arrives along the great circle path. The azimuth versus slowness plots (C and D) can detect signals generated at interfaces dipping as steeply as 30° [*Castle and Creager*, 1998].

[17] These synthetic seismograms model the $S_{1700}P$ phase generated by a 2% V_s change, including attenuation. $S_{1700}P$ is easily seen in both the vespegram and in the back-azimuth/slowness plot (Figure 3), suggesting that a 2% V_s

change should be visible in the data. Complete synthetics show that vespegrams can detect *S*-to-*P* conversions off of the 660-km discontinuity with a ΔV_s as small as 1% [*Castle and Creager*, 1997]. [*Niu and Kawakatsu*, 1997] use data from California seismic arrays to detect discontinuities near 1000 km with ΔV_s as low as 0.5%. Obviously, as modeled in our synthetics, the *S*-to-*P* conversions that occur at greater depth encounter more attenuation along the longer *S* leg. Additionally, *van der Lee et al.* [1994] and *Castle and Creager* [2000] show that discontinuity topography can both magnify and reduce seismic amplitudes, depending critically on the curvature of the seismic interface. We examined data from many earthquakes to reduce the likelihood that interface curvature affected all of our results.

4. Results

[18] We have examined PNSN records of deep earthquakes for signs of *S*-to-*P* conversions S_XP at structures between 800 and 2000 km depth. Data from other dense networks exist, for instance in Japan, but for this study we chose PNSN because it is a large aperture (roughly 1000 km north-south), dense network (over 140 stations) that has been operating since the early 1980s and the data are easily available from the Incorporated Research Institutions for Seismology Data Management Center (IRIS DMC). From the [*Engdahl et al.*, 1998] hypocenter catalog, we chose earthquakes with $m_b \geq 5.5$, at distances between 55° and 90°, and at depths ≥500 km. For smaller distances the *P* and *S* waves do not reach 1700 km depth so that reflected waves can be used [*Castle and van der Hilst*, 2000, also manuscript in preparation, 2002] but not S_XP. At depths less than 500 km, the *pP* phase arrives earlier than an *S*-to-*P* conversion at 1700 km and the *pP* coda can mask later arrivals. The search for deeper structures also requires a well recorded *P* wave and a recorded time window of at least 120 s. The 46 earthquakes which meet these requirements lie in four regions: the Marianas, the northwest Pacific, South America, and Tonga/Fiji (Table 1 and Figure 4).

4.1. Marianas

[19] The three events in the northern Marianas region (Table 1, earthquakes 1, 2, and 3, Figure 5) all show an arrival at ~85 s, near the theoretical time of $S_{1700}P$ but at a different slowness and back-azimuth than predicted for an *S*-to-*P* conversion off of a horizontal structure at 1700 km. Explanations for these arrivals are either *P*-to-*P* reflections off a dipping structure in the upper mantle [*Wicks and Weber*, 1996] or *S*-to-*P* conversions off either a point scatterer [*Kaneshima and Helffrich*, 1998] or a dipping surface [*Kaneshima and Helffrich*, 1999] in the lower mantle. That the phase arrives earlier from deeper earthquakes than from shallower earthquakes argues that it is an *S*-to-*P* conversion off of a structure beneath the earthquakes [*Kaneshima and Helffrich*, 1998]. That the signal is seen from earthquakes in several locations in the northern Marianas region [*Kaneshima and Helffrich*, 1999] and that we also observe the phase in records of shallow earthquakes in the middle and southern Marianas regions (not shown) suggests that the structure is not a point source but rather a dipping structure at depths ranging from 1500 to 1800 km. That the structure is nonhorizontal also explains the observed variations in slowness and back-azimuth. Finally, the scatterer location lies within a broad fast region in *S*-wave tomographic models [*Grand et al.*, 1997], somewhat suggestive of a connection between the scatterer and subducted material.

Figure 4. A map of the study regions. Crosses mark earthquake locations; red circles mark hypothetical *S*-to-*P* conversion locations at 1700 km depth; green triangles mark station locations in the PNSN; and blue lines mark plate boundaries.

[20] In addition to the $S_{1700}P$ phase, arrivals exist at ~20 s (earthquakes 1 and 2), 30 s (event 1), and 55 s (event 3). The energy at 55 s in earthquake 3 is well constrained in both time and slowness and is most likely $s_{420}P$. The arrivals at 20 s may be $S_{800}P$; however, the arrival time is earlier for the shallower earthquake (event 2), implying that arrival is an upgoing phase such as $s_{550}P$ or $p_{500}P$. The arrival at 30 s in earthquake 1 could be $p_{420}P$. Arrivals at 42 s and 48 s are likely $s_{420}P$ and $S_{1200}P$. Earthquake 3 shows signs of $S_{1250}P$ and $S_{1550}P$. These phases are difficult to interpret due to their inconsistent observation and could be the result of an aftershock.

4.2. Northwest Pacific

[21] Seven earthquakes in the northwest Pacific were deeper than 500 km and well recorded at PNSN (Figure 6). Earthquakes 4, 8, and 9 all show energy arriving at the slowness and time expected for $S_{1200}P$. However, the other earthquakes show no signs of a horizontal 1200-km discontinuity. An arrival near 30 s in earthquake 4 may be $p_{390}P$. Other arrivals in earthquake 4 near 20 s could be either upgoing reflected phases or downgoing converted phases. Because they are not seen in other events we do not interpret them.

[22] Energy that arrives along azimuths off the great circle path between earthquake and receiver will not appear in the vespegrams but may be imaged in the back-azimuth versus slowness plots. Searching through these plots, earthquakes 4 and 7 show energy arriving off the great path at a

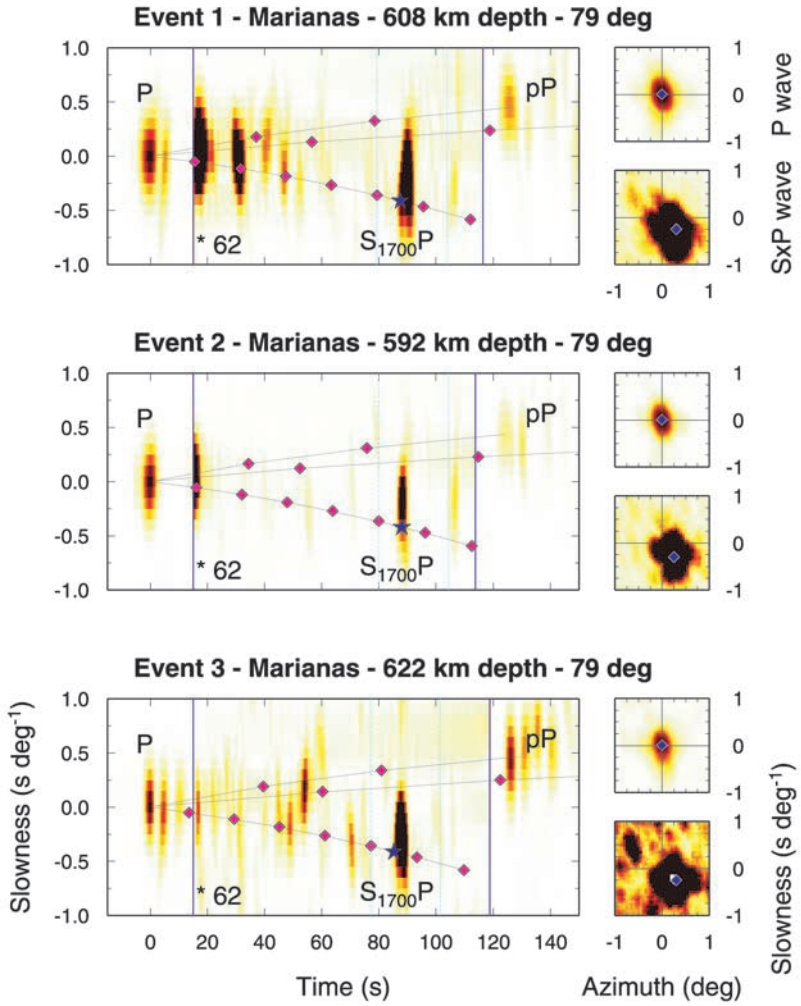

Figure 5. Vespegrams and back-azimuth/slowness plots for Marianas events. The vespegrams plot the slowness and time of energy arriving at one back-azimuth (the great circle path), while the back-azimuth/slowness plots plot the back-azimuth and slowness of energy arriving at the predicted P time (top) and S_XP time (bottom). For other symbols, see caption of Figure 3.

small slowness in the time window expected for an S-to-P conversion at depths between 1600 and 1900 km. This observation is not repeated in data from other earthquakes. In fact, recordings of earthquakes 5, 6, 8, 9, and 10 suggest that the depth interval 1600 km to 2000 km is largely devoid of structure in the northwest Pacific.

4.3. South America

[23] Earthquakes 11–22 occurred beneath South America (Figure 7). Earthquakes 16 and 20 show several arrivals but both earthquakes had long solar time functions which make signal identification difficult (e.g., the two pulses in the first few seconds of earthquake 16). Earthquake 20 is, in fact, the large, deep Bolivian earthquake that occurred in June 1996, and lasted almost 1 min. The distinct arrival at ~80 s in earthquake 11 could be S_XP off of a dipping surface at 1500 km. Other possible signatures in earthquake 11 include $p_{300}P$ (30 s) and $s_{450}P$ (20 s). Earthquake 17 includes a potential $S_{1300}P$ (20 s). Earthquakes 12 and 18 show weak, but coherent energy arriving along non-great circle paths that could be generated at structures between 1600 and 1900 km depth. Unfortunately, the difference in slowness between upgoing and downgoing phases is very small at 90° distance such that these phases could also be reflected upgoing energy. However, earthquakes 13, 14, 15, 17, 19, 21, and 22 all show no energy arriving in the 1600 km to 2000 km time range.

4.4. Tonga/Fiji

[24] With 24 well-recorded, deep earthquakes we have the most data from the Tonga/Fiji region (Figures 8 and 9). Several recordings show energy in the vespegrams: earthquakes 24, 29, 31, 33, 34, and 37 and possibly earthquakes 28 and 32. Earthquakes 24, 29, 31, 32, and 34 all shows signs of the $p_{410}P$ phase and questionably a $s_{410}P$ in earthquake 31. Earthquakes 29 and 33 both have a $S_{1300}P$ arrival while earthquakes 28 and 37 may have $S_{1500}P$ arrivals. Coherent arrivals exist along non-great circle paths at $S_{1600}P$ to $S_{1900}P$ times for earthquakes 27, 29, 31, and possibly 37 at slownesses less than P and for earthquakes 32, 33, 34, 45, and possibly earthquake 26 at slownesses greater than P.

[25] More striking than the sporadically occurring arrivals is the number of Tonga/Fiji earthquakes that show no later arrivals, even at this extreme amplification. In fact, the

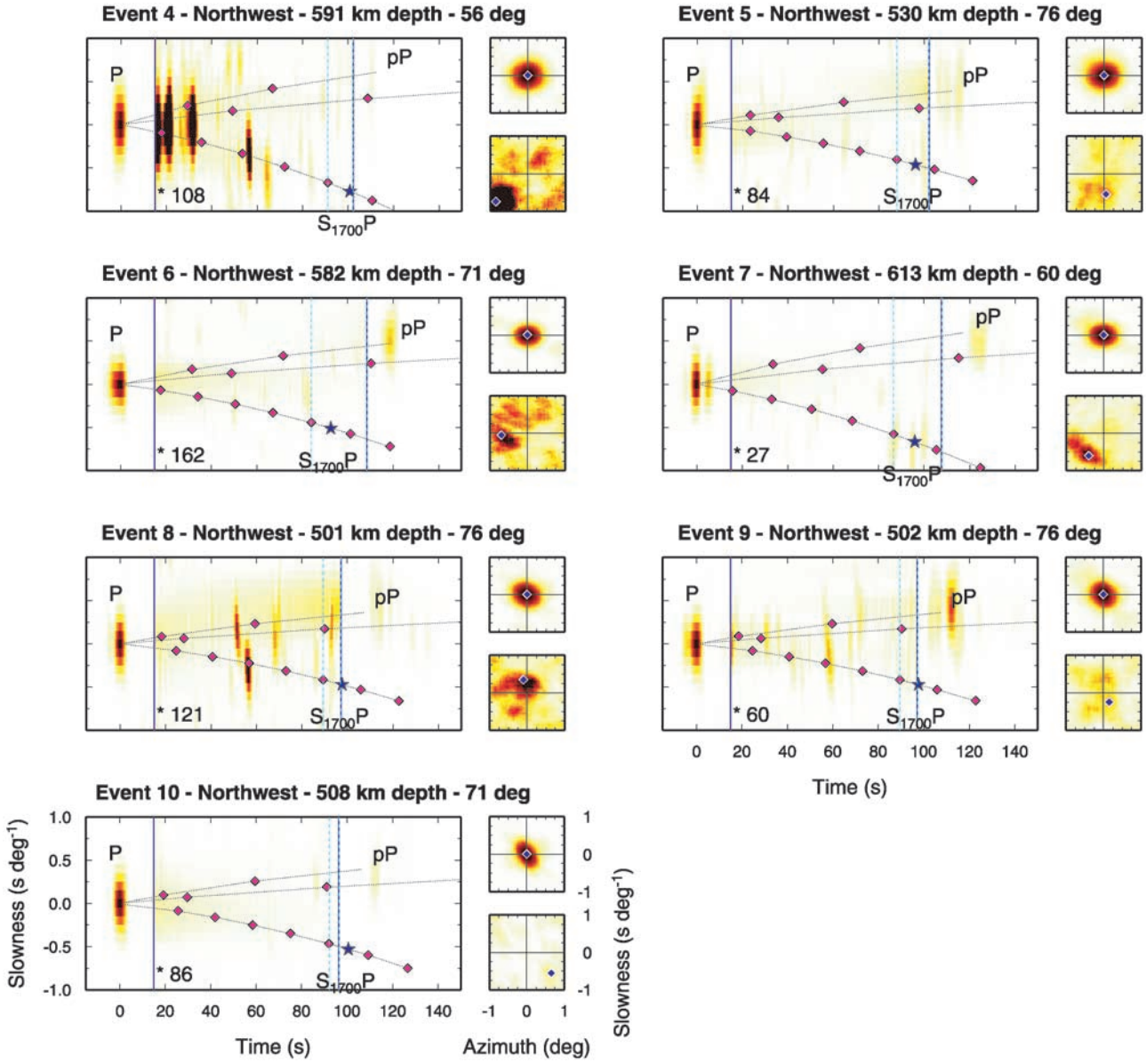

Figure 6. Vespegrams and back-azimuth/slowness plots for the northwest Pacific earthquakes. See caption of Figure 3.

majority of Tonga/Fiji earthquakes (events 23, 25, 28, 30, 35, 36, 38, 39, 40, 41, 42, 43, 44, and 46) show no signs of later arrivals generated at depths between 1600–2000 km depth. For example, earthquake 41 produced records that, even with significant amplification, do not reveal $s_{410}P$, $p_{410}P$, or any downgoing S-to-P conversions. Such observations are difficult to reconcile with a global seismic discontinuity or thermal boundary layer in the depth range 800 to 2000 km.

5. Discussion

[26] We found several "410-km" arrivals ($s_{410}P$ and $p_{410}P$), one possible $S_{800}P$, one possible $S_{1200}P$, two possible $S_{1300}P$, and three possible $S_{1500}P$. We confirmed previous observations of $S_{1600}P$ in the Marianas regions. Outside of Marianas, 14 of 43 earthquakes showed possible signs of S-to-P conversions in the 1600–1900 km depth range, but not all of this evidence is unequivocal. In well studied regions such as Izu-Bonin and Tonga/Fiji, $S_{660}P$ can be seen over 80% of the time [e.g., *Wicks and Richards*, 1993; *Niu and Kawakatsu*, 1995; *Castle and Creager*, 1998]. The $S_{660}P$ is not observed in the data considered here because the earthquakes are so deep that little time separation occurs between the P wave and $S_{660}P$. A small percentage of the records processed in this study show signals reflected off the underside of the 410-km discontinuity. Our difficulty in imaging reflected $p_{410}P$ is consistent with the difficulties reported in previous detailed studies of the 410-km discontinuity [*Collier and Helffrich*, 1997].

[27] A global discontinuity at 920 km was proposed based on high quality observations sampling beneath Indonesia [*Kawakatsu and Niu*, 1994] and additional observations in other subduction zones [*Niu and Kawakatsu*, 1997]. While

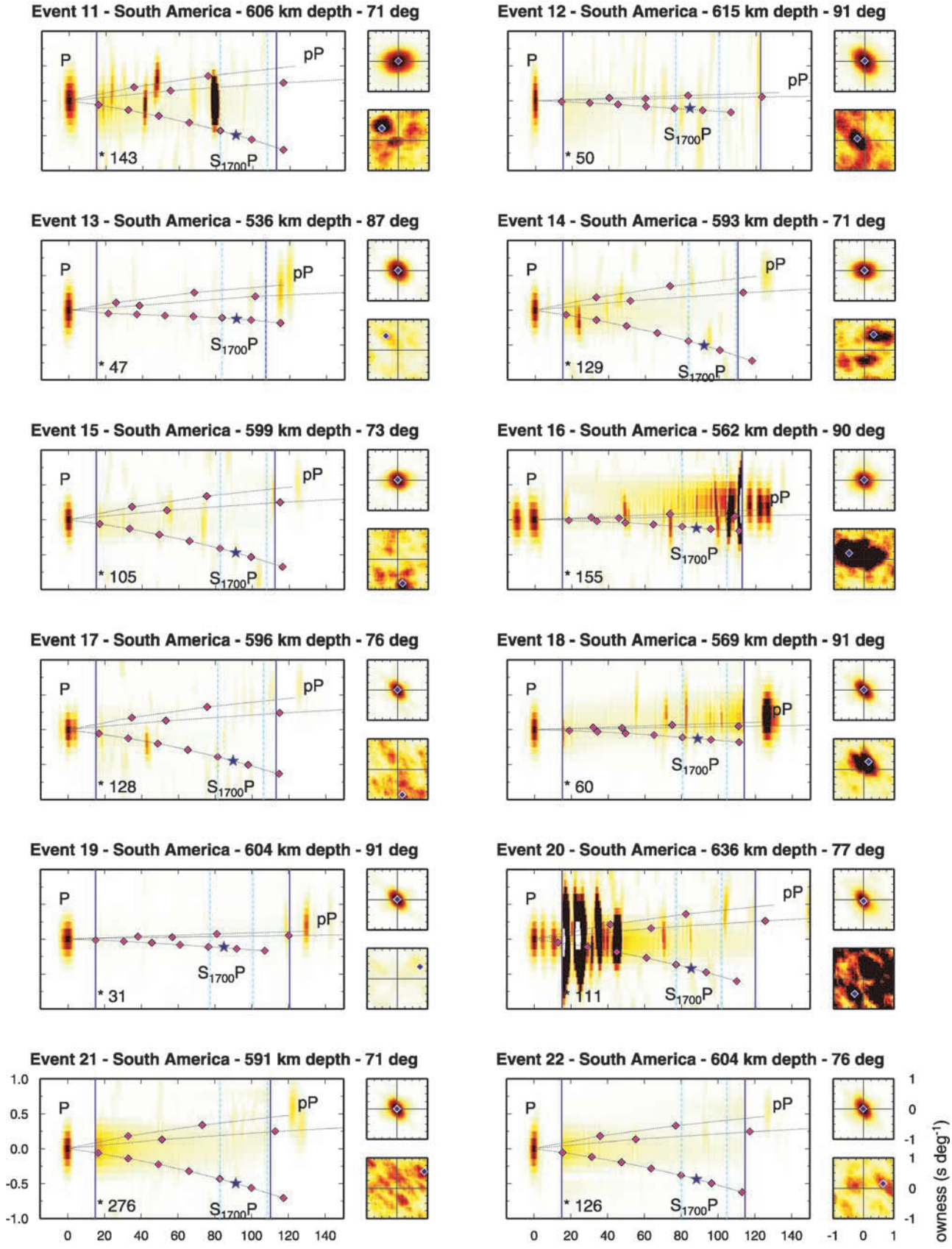

Figure 7. Vespegrams and back-azimuth/slowness plots for the South America earthquakes. See caption of Figure 3.

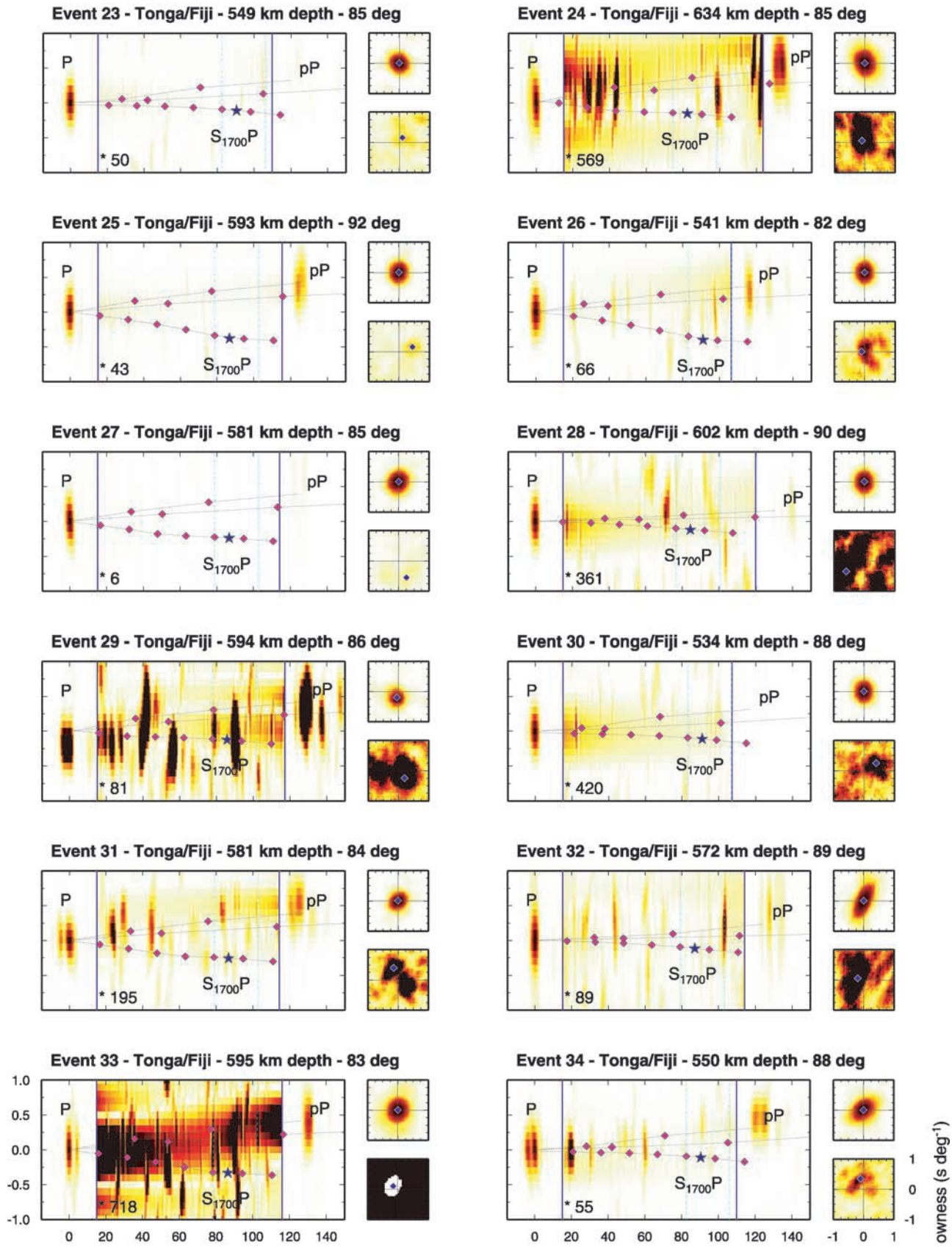

Figure 8. Vespegrams and back-azimuth/slowness plots for the Tonga/Fiji earthquakes (events 23–34). See caption of Figure 3.

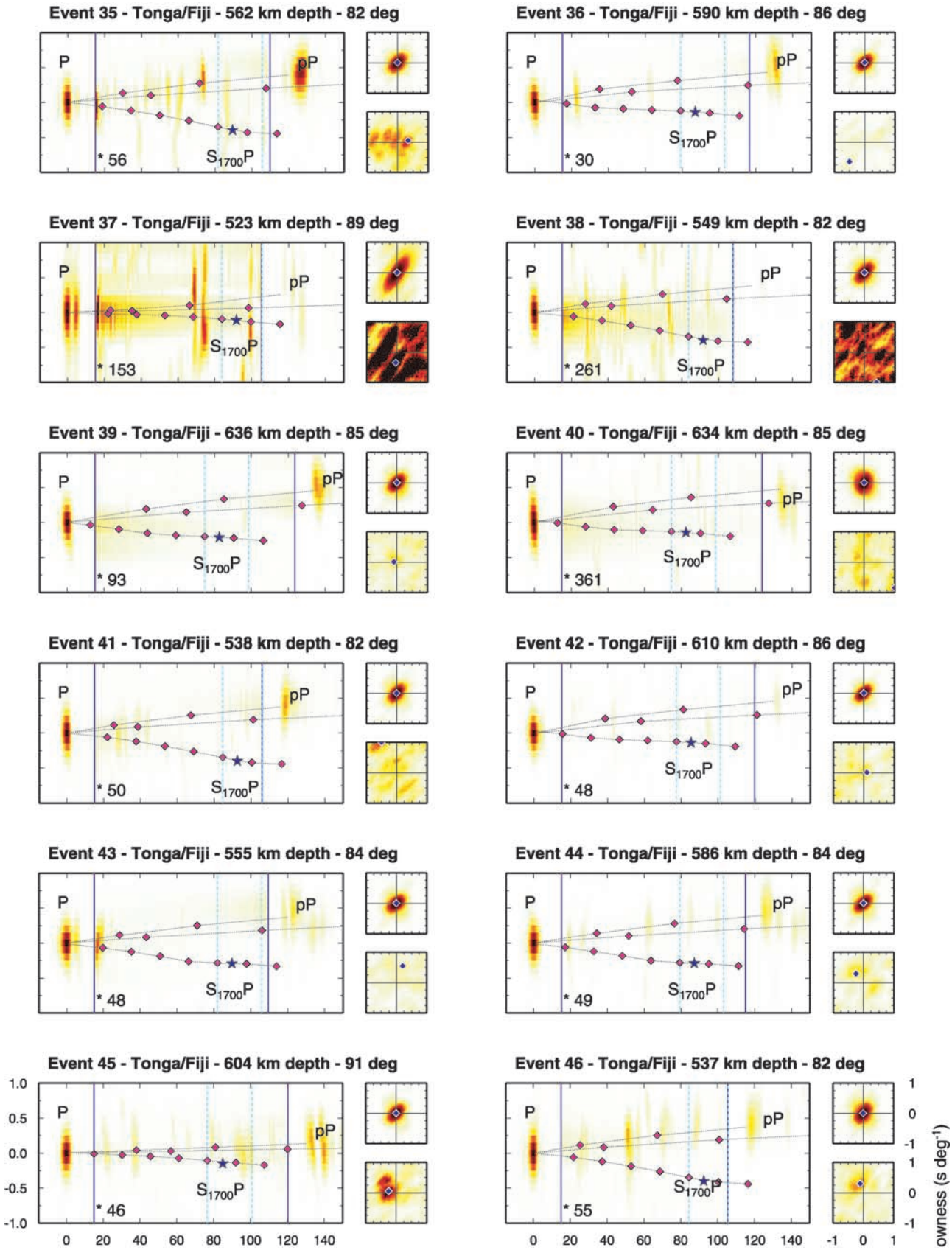

Figure 9. Vespegrams and back-azimuth/slowness plots for the Tonga/Fiji earthquakes (events 35–46). See caption of Figure 3.

we observe occasional signals that could be attributed to a discontinuity near 1000km, we do not find convincing evidence in the regions studied here. Thus, we feel the 920-km discontinuity should be interpreted either as a structure local to the Indonesian subduction complex or a global discontinuity with either a variable transition thickness or ΔV_s.

[28] Data from Marianas earthquakes show signs of a deep structure in the middle mantle. However, earthquakes from other regions do not consistently show arrivals from this deep structure. In fact, the lower mantle from 800 to 2000 km depth appears to be one of the smoother areas in the mantle, arguing against a mineralogical phase change or compositional boundary in this depth range below the convergent margins studied here.

[29] Can we conclude from this that no deep compositionally distinct and geochemically enriched reservoir exist? Three questions arise: First, could the interface between chemical reservoirs be smooth and thus undetectable by short period data? Second, could the wave speed change at the interface be too small to detect? Third, could the morphology of the deep layer prevent detection by our method and data coverage?

5.1. Sharpness of an Interface

[30] How abruptly do we expect the material properties to change (i.e., the sharpness of the discontinuity) at the transition between two chemical reservoirs? Attempting to explain the observed sharpness of the 660-km discontinuity, *Lees et al.* [1983] stated that an interface between compositionally distinct reservoirs would be extremely sharp, with most changes occurring over less than 5 km. Unless a gradient can somehow be sustained dynamically with an equilibrium between replenishment and erosion, a more gradual transition from one reservoir into another would allow more entrainment of the two reservoirs into each other, providing less resistance to mixing and calling into question the long term stability of the layers. Reservoir stability and resistance to entrainment comes either from the inherent rheological properties of blobs [*Becker et al.*, 1999] or from a density increase in a lower layer which dynamically resists flow to shallower depths [*Sleep*, 1988; *Tackley*, 1998; *Kellogg et al.*, 1999a, 1999b; *Davaille*, 1999]. However, as the density contrast increases, the dynamic topography on the boundary decreases, which should increase the seismic visibility of the boundary in global stacks. Global stacks of seismic data do not reveal signals from a discontinuity in this depth range. Thus, while an increase in topography on the boundary will decrease its visibility, the increase in topography also implies a smaller density increase and therefore, problematically, less resistance to mixing.

[31] At the seismic frequencies used here, synthetics show that a smooth but abrupt velocity change with a transition width greater than 20 km passes largely undetected. We did identify sharp interfaces, which we define here as a boundary for which a significant part of the wave speed change occurs over less than 20 km, in the depth range 800–2000 km, but these signals were localized and infrequent.

5.2. Wave Speed Change at a Boundary

[32] An enriched lower layer with a sharp but seismically invisible interface could exist if the wave speed change across the boundary is small. If this is the case, then our observations suggest that the shear wave contrast at the boundary would be less than the detection level in all areas except the Marianas. The model proposed by *Kellogg et al.* [1999a] also implies that slab debris can accumulate atop the deep layer, but, again with the possible exception of the Marianas, our data do not provide evidence for this.

[33] Discussions of the chemical difference between the different reservoirs have revolved on enrichment in either iron or silicon, or both. Iron enrichment primarily increases the density, which decreases the wave speeds, while a silicon enrichment mainly affects the perovskite/magnesiowüstite partitioning, increasing the amount of perovskite and increasing velocities [*Kellogg et al.*, 1999a].

[34] Tomographic images of slabs reveal sheet-like planar features descending from subduction zones to the base of the mantle. However images of fast slab-like anomalies are least apparent within the depth range 1700–2200 km, even in well resolved regions [e.g., *van der Hilst et al.*, 1997; *van der Hilst and Kárason*, 1999; *Kárason and van der Hilst*, 2001], possibly because wave speeds may be less sensitive to temperature in this depth range. An iron enrichment in the ambient mantle near 1700 km depth would decrease wave speeds in the lower layer and thus increase the wave speed contrast between a descending slab and the surrounding mantle. These observations in conjunction with the results of this study suggest that a lower layer must be enriched in both iron and silicon: enriched in iron to increase its density, providing long term stability, and enriched in silicon to create a smaller velocity change, preventing detection by scattered waves, and reducing the velocity contrast between slabs and lower mantle.

5.3. Morphology of the Interface

[35] An unfavorable orientation (dip >30°) of the interface would make it harder to detect even when marked by a sharp change in properties [*Castle and Creager*, 1998]. Furthermore, an interface at a depth greater than 2000 km would remain undetected with the approach used here. We have studied mantle regions beneath downwellings where some numerical and analog modeling of chemically distinct reservoirs has shown that a compositional boundary would be depressed and prone to large topography [*Davaille*, 1999]. The topography would limit our detection capability and, depending on the ''ambient'' depth of the interface, the boundary could be depressed out of our depth detection limit.

6. Concluding Remarks

[36] In only one of the four regions that we investigated did we find convincing evidence for structure between 800 and 2000 km depth. From this we conclude that it is unlikely that a global interface exists between 800 and 2000 km depth that is sharp (<20 km), subhorizontal (slope of <30°), and associated with a large wave speed contrast (>2%). This result is in agreement with that of [*Vidale et al.*, 2001].

[37] A lower layer of enriched material could extend into this depth range if the boundary between the depleted and enriched layers is either a diffuse boundary or has a small wave speed change. A convecting mantle most likely causes mixing across a diffuse boundary, which would eliminate

chemical separation between the layers, unless a gradient in material properties can be sustained dynamically [*Albarède and van der Hilst*, 2002]. Preliminary calculations [*Kellogg et al.*, 1999a] suggest enrichment in both iron and silicon could render the compositionally distinct domains to be almost seismically invisible. Second, on the basis of the model proposed by [*Kellogg et al.*, 1999a], one potential scenario is that an anomalous deep mantle layer, if it exists, is depressed or even absent beneath major downwellings. However, limiting the volume containing the radiogenically enriched material too much would potentially raise the layer temperature near either its solidus or its destabilizing temperature. Unfortunately, owing to the geographic distribution of sources and dense receiver arrays only regions underneath convergent margins have been investigated with our approach or that of [*Vidale et al.*, 2001], while large regions of the mantle have remained unexplored by such techniques. Data coverage poses limitations to the application of this method and we strongly prod seismic data centers to make all of their short-period data as easily available to the seismic community as the PNSN data are available through IRIS.

[38] **Acknowledgments.** Discussions with Ken Creager were fruitful. Figures were created with GMT [*Wessel and Smith*, 1995]. This research was supported by the National Science Foundation (EAR9814614) and we thank IRIS. We thank Frederik Simons for his assistance with Latex and Justin Revenaugh help a critical review. Part of this manuscript was written when R.v.d.H. visited the Institut de Physique du Globe de Paris.

References

Albarède, F., and R. D. van der Hilst, New mantle convection model may reconcile conflicting evidence, *Eos Trans. AGU*, *80*, 535, 537–539, 1999.

Albaréde, F., and R. D. van der Hilst, Zoned mantle convection, *Philos. Trans. R. Soc. London Math. Phys. Eng. Sci.*, *361*, in press, 2002.

Becker, T. W., J. B. Kellog, and R. J. O'Connell, Thermal constraints on the survival of primitive blobs in the lower mantle, *Earth Planet. Sci. Lett.*, *171*, 351, 1999.

Castle, J. C., and K. C. Creager, Seismic evidence against a mantle chemical discontinuity near 660 km depth beneath Izu-Bonin, *Geophys. Res. Lett.*, *24*, 241–244, 1997.

Castle, J. C., and K. C. Creager, Topography of the 660-km discontinuity beneath Izu-Bonin: Implications for tectonic history and slab deformation, *J. Geophys. Res.*, *103*, 12,511–12,528, 1998.

Castle, J. C., and K. C. Creager, A steeply dipping discontinuity in the lower mantle beneath Izu-Bonin, *J. Geophys. Res.*, *104*, 7279–7292, 1999.

Castle, J. C., and K. C. Creager, Local sharpness and shear wave velocity jump across 660-km discontinuity, *J. Geophys. Res.*, *105*, 6191–6200, 2000.

Castle, J. C., and R. D. van der Hilst, The core-mantle boundary under the Gulf of Alaska: No ULVZ for shear waves, *Earth Planet. Sci. Lett.*, *176*, 311–321, 2000.

Chapman, C. H., J. Chu, and D. G. Lyness, The WKBJ seismogram algorithm, in *Seismologial Algorithms*, edited by D. J. Doornbos, p. 47, Academic, San Diego, Calif., 1988.

Christensen, U. R., and A. W. Hofmann, Segregation of subducted oceanic crust in the convecting mantle, *J. Geophys. Res.*, *99*, 19,867–19,884, 1994.

Collier, J., and G. Helffrich, Topography of the "410" and "660" km seismic discontinuities in the Izu-Bonin subduction zone, *Geophys. Res. Lett.*, *24*, 1535–1538, 1997.

Creager, K. C., and T. H. Jordan, Slab penetration into the lower mantle beneath the Mariana and other island arcs of the northwest Pacific, *J. Geophys. Res.*, *91*, 3573–3589, 1986.

Davaille, A., Simultaneous generation of hotspots and superswells by convection in a heterogenous planetary mantle, *Nature*, *402*, 756–760, 1999.

Davies, G. F., Geophysically constrained mantle mass flows and the Ar-40 budget: A degassed lower mantle?, *Earth Planet. Sci. Lett.*, *166*, 149–162, 1999.

Dziewonski, A., and D. L. Anderson, Preliminary reference Earth model, *Phys. Earth Planet. Inter.*, *25*, 297–356, 1981.

Engdahl, E. R., R. D. van der Hilst, and R. P. Buland, Global teleseismic earthquake relocation with improved travel times and procedures for depth determination, *Bull. Seismol. Soc. Am.*, *88*, 722–743, 1998.

Forte, A. M., and J. X. Mitrovica, Deep-mantle high-viscosity flow and thermochemical structure inferred from seismic and geodynamic data, *Nature*, *41*, 1049–1056, 2001.

Grand, S. P., R. D. van der Hilst, and S. Widiyantoro, Global seismic tomography: A snapshot of convection in the Earth, *GSA Today*, *7*, 1–7, 1997.

Hedlin, R. A. H., P. M. Sheaer, and P. S. Earle, Seismic evidence for small-scale heterogeneity throughout the Earth's mantle, *Nature*, *387*, 145–150, 1997.

Hofmann, A. W., Mantle geochemistry: The message from oceanic volcansim, *Nature*, *385*, 219–229, 1997.

Kaneshima, S., and G. Helffrich, Detection of lower mantle scatterers northeast of the Mariana subduction zone using short-period array data, *J. Geophys. Res.*, *103*, 4825–4838, 1998.

Kaneshima, S., and G. Helffrich, Dipping low-velocity layer in the mid-lower mantle: Evidence for geochemical heterogeneity, *Science*, *283*, 1888–1891, 1999.

Kárason, H., and R. D. van der Hilst, Tomographic imaging of the lowermost mantle with differential times of refracted and diffracted core phases (*PKP*, P_{diff}), *J. Geophys. Res.*, *106*, 6569–6588, 2001.

Kawakatsu, H., and F. L. Niu, Seismic evidence for a 920-km discontinuity in the mantle, *Nature*, *371*, 301–305, 1994.

Kellogg, L. H., B. H. Hager, and R. D. van der Hilst, Compositional stratification in the deep mantle, *Science*, *283*, 1881–1884, 1999a.

Kellogg, L. H., D. L. Hunt, B. H. Hager, and S. Zhong, Dynamics of a hot abyssal layer in the mantle (abstract), *Eos Trans. AGU*, *77*(46), Fall Meet. Suppl., F31, 1999b.

Kennett, B. L. N., and E. R. Engdahl, Travel times for global earthquake location and phase identification, *Geophys. J. Int.*, *105*, 429–465, 1991.

Kennett, B. L. N., E. R. Engdahl, and R. Buland, Constraints on seismic velocities in the Earth from traveltimes, *Geophys. J. Int.*, *122*, 108–124, 1995.

Kennett, B. L. N., S. Widiyantoro, and R. D. van der Hilst, Joint seismic tomography for bulk sound and shear wave speed in the Earth's mantle, *J. Geophys. Res.*, *103*, 12,469–12,493, 1998.

Lees, A. C., M. S. T. Bukowinski, and R. Jeanloz, Reflection properties of phase transition and compositional change models of the 670-km discontinuity, *J. Geophys. Res.*, *88*, 8145–8159, 1983.

Masters, G. H., G. Laske, H. Bolton, and A. M. Dziewonski, The relative behavior of shear velocity, bulk sound speed, and compressional velocity in the mantle: Implications for chemical and thermal structure, in *Earth's Deep Interior: Mineral Physics and Tomography From the Atomic to the Global Scale*, *Geophys. Monogr. Ser.*, vol. 117, pp. 63–87, edited by G. M. et al., AGU, Washington, D. C., 2000.

Niu, F., and H. Kawakatsu, Direct evidence for the undulation of the 660-km discontinuity beneath Tonga: Comparision of Japan and California array data, *Geophys. Res. Lett.*, *22*, 531–534, 1995.

Niu, F., and H. Kawakatsu, Depth variation of the mid-mantle seismic discontinuity, *Geophys. Res. Lett.*, *24*, 429–432, 1997.

Revenaugh, J., and T. H. Jordan, Mantle layering from ScS reverberations, 4, The lower mantle and core-mantle boundary, *J. Geophys. Res.*, *96*, 19,811–19,824, 1991.

Saltzer, R. L., R. D. van der Hilst, and H. Karason, Comparing *p* and *s* wave heterogeneity in the mantle, *Geophys. Res. Lett.*, *28*, 1335–1338, 2001.

Schimmel, M., and H. Paulssen, Noise reduction and detection of weak, coherent signals through phase-weighted stacks, *Geophys. J. Int.*, *130*, 497–505, 1997.

Shearer, P. M., Imaging global body-wave phases by stacking long-period seismograms, *J. Geophys. Res.*, *96*, 20,353–20,364, 1991.

Sipkin, S., Estimation of earthquake source parameters by the inversion of waveform data: Global seismicity, *Bull. Seismol. Soc. Am.*, *76*, 1515–1541, 1986.

Sleep, N. H., Gradual entrainment of a chemical layer at the base of the mantle by overlying convection, *Geophys. J.*, *95*, 437–447, 1988.

Tackley, P. J., Three-dimensional simulations of mantle convection with a thermo-chemical basal boundary layer: D″?, in *The Core-Mantle Boundary Region*, *Geodyn. Ser.*, vol. 28, edited by M. G. et al., pp. 231–253, AGU, Washington, D. C., 1998.

Tackley, P. J., Mantle convection and plate tectonics: Toward an integrated physical and chemical theory, *Science*, *288*, 2002–2007, 2000.

van der Hilst, R. D., and H. Kárason, Compositional heterogeneity in the bottom 1000 km of the Earth's mantle: Toward a hybrid convection model, *Science*, *283*, 1885–1888, 1999.

van der Hilst, R. D., S. Widiyantoro, and E. R. Engdahl, Evidence for deep mantle circulation from global tomography, *Nature*, *386*, 578–584, 1997.

van der Hilst, R. D., S. Widiyantoro, K. C. Creager, and T. J. McSweeney, Deep subduction and aspherical variations in *P*-wavespeed at the base of

Earth's mantle, in *The Core-Mantle Boundary Region*, *Geodyn. Ser.*, vol. 28, edited by M. G. et al., pp. 5–20, AGU, Washington, D. C., 1998.

van der Lee, S., H. Paulssen, and G. Nolet, Variability of *P*660*s* phases as a consequence of topography of the 660 km discontinuity, *Phys. Earth Planet. Inter.*, *86*, 147–164, 1994.

Vidale, J. E., G. Schubert, and P. S. Earle, Unsuccessful initial search for a midmantle chemical boundary with seismic arrays, *Geophys. Res. Lett.*, *28*, 859–862, 2001.

Vinnik, L., S. Chevrot, and J. P. Montagner, Evidence for a stagnent plume in the transition zone, *Geophys. Res. Lett.*, *24*, 1007–1010, 1997.

Wessel, P., and W. H. F. Smith, New version of the Generic Mapping Tools released, *Eos Trans. AGU*, *76*, 329, 1995.

White, W. M., and A. W. Hofmann, Mantle heterogeneity and isotopes in oceanic basalts, *Nature*, *295*, 363–364, 1982.

Wicks, C. W., Jr., and M. A. Richards, A detailed map of the 660-kilometer discontinuity beneath the Izu-Bonin subduction zone, *Science*, *261*, 1424–1427, 1993.

Wicks, C. W., Jr., and M. Weber, California broadband array evidence for an upper mantle reflector beneath the west Mariana ridge, *Eos Trans. AGU*, *77*(46), Fall Meet. Suppl., F492, 1996.

J. C. Castle, Rosetta Inpharmatics/Merck, 12016 115th Ave NE, Kirkland, WA 98034, USA. (jccastle@yahoo.com)

R. D. van der Hilst, Department of Geophysics, Institute of Earth Sciences Utrecht University, Budapestlaan 4, 3508 TA Utrecht, Netherlands. (hilst@geo.uu.nl)